

# Analysis of 3D Anisotropic Solids Using Fundamental Solutions Based on Fourier Series and the Adaptive Cross Approximation Method

R. Q. Rodríguez<sup>1,2</sup>, C. L. Tan<sup>2</sup>, P. Sollero<sup>1</sup> and E. L. Albuquerque<sup>3</sup>

**Abstract:** The efficient evaluation of the fundamental solution for 3D general anisotropic elasticity is a subject of great interest in the BEM community due to its mathematical complexity. Recently, Tan, Shiah, and Wang (2013) have represented the algebraically explicit form of it developed by Ting and Lee (Ting and Lee, 1997; Lee, 2003) by a computational efficient double Fourier series. The Fourier coefficients are numerically evaluated only once for a specific material and are independent of the number of field points in the BEM analysis. This work deals with the application of hierarchical matrices and low rank approximations, applying the Adaptive Cross Approximation (ACA) to treat 3D general anisotropic solids in BEM using this Green's function based on Fourier series. The use of hierarchical format is aimed at reducing the storage requirements of the system matrices and the computational effort in the BEM analysis of large systems. Numerical examples are presented to show the successful implementation of using ACA and the formulation based on Fourier series for BEM analysis of 3D anisotropic solids.

**Keywords:** Adaptive Cross Approximation, Boundary Element Method, Hierarchical Matrices, Anisotropic Fundamental Solution, Fourier Series.

## 1 Introduction

The evaluation of the fundamental solution and its derivatives is a necessary step in the direct BEM formulation. The efficient and accurate computation of these quantities is a concern for the case of 3D general anisotropic solids because of their mathematical complexity. Also, for very large numerical problems, the fully populated and non-symmetric system matrices impose relatively high memory requirements and high solution times. This work deals with these two issues, the fun-

---

<sup>1</sup> Faculty of Mechanical Engineering, University of Campinas, Brazil.

<sup>2</sup> Department of Mechanical and Aerospace Engineering, Carleton University, Canada.

<sup>3</sup> Faculty of Technology, University of Brasilia, Brazil.

damental anisotropic solution and the speed-up of the BEM process. Fundamental solutions for 2D and 3D isotropic elastostatics can be represented in relatively simple explicit forms. That is not the case for general anisotropic solids, particularly in 3D. Ting and Lee [Ting and Lee (1997); Lee (2003)] have derived exact, explicit expressions for the fundamental solution and its derivatives. However, the presence of high-order tensors and highly complex mathematical expressions for the derivatives, although straightforward to implement, may be less than ideal for very efficient computations. These solutions were first implemented into a BEM code by Tan, Shiah, and Lin (2009). More recently, these authors have expressed this Green's function and its derivatives by a double Fourier Series [Tan, Shiah, and Wang (2013); Shiah, Tan, and Wang (2012)], demonstrating the much superior efficiency for their computations, and the relative simplicity of their implementation. Many research studies have, in recent years, also focused on improving the solution process in BEM [Rokhlin (1985); Bebendorf (2000); Bebendorf and Rjasanow (2003); Wang, Yao, and Lei (2006); Wang, Zhu, and Zhang (2012)]. Bebendorf and Rjasanow (2003), for example, suggested the use of purely algebraic algorithms to generate the approximation of suitable blocks of the collocation matrix from only a few entries of the original blocks. This technique is referred to as the Adaptive Cross Approximation (ACA). The ACA uses matrix hierarchization to reduce the storage requirement and the computational effort in the BEM analysis. Several works have applied the ACA to accelerate the BEM process. Brancati, Aliabadi, and Benedetti (2009) applied the ACA with a GMRES solver to acoustic problems and called the method Rapid Acoustic Boundary Element Method (RABEM). Brancati, Aliabadi, and Milazzo (2011) modified and improved the ACA to account for sound absorbent materials. Their new approach is shown to be 50% faster in CPU time than the conventional ACA. More recently, Yoshikawa, Matsumura, and Nishimura (2013) have also applied the ACA to the time domain boundary integral equation method (TD-BIEM) using the Lubich convolution quadrature method (CQM) while Wang and Yao (2013) applied the ACA to 3D dynamic analysis of a HTR-PM (High Temperature Reactor - Pebble Module). In this paper, the application of hierarchical matrices and ACA for treating 3D anisotropic solids using BEM with the fundamental solution based on double Fourier series is illustrated. In what follows, the anisotropic fundamental solution and its derivatives are first reviewed. The use of hierarchical matrices and ACA is then briefly discussed before numerical examples are presented.

## 2 3D fundamental solution for displacements and its derivatives in anisotropic elasticity

The 3D fundamental solution for a generally anisotropic material can be expressed in terms of the Barnett-Lothe tensor  $\mathbf{H}[\mathbf{x}]$ , see, e.g., Ting and Lee (1997). The Barnett-Lothe tensor could also be expressed in spherical coordinates as follows,

$$\mathbf{U}(r, \theta, \phi) = \frac{1}{4\pi r} \mathbf{H}(\theta, \phi) \tag{1}$$

where  $r$  represents the radial distance between the source and the field points. As this expression depends only on the spherical angles  $(\theta, \phi)$ , it can be expressed in terms of the Stroh's eigenvalues as

$$\mathbf{H}(\theta, \phi) = \frac{1}{|\mathbf{T}|} \sum_{n=0}^4 q_n \hat{\Gamma}^{(n)} \tag{2}$$

The explicit expressions for  $|\mathbf{T}|$ ,  $\hat{\Gamma}^{(n)}$  and  $q_n$  can be found in Ting and Lee (1997); Tan, Shiah, and Wang (2013). Due to its periodic nature,  $\mathbf{H}(\theta, \phi)$  can be expressed as double Fourier series around  $\theta$  and  $\phi$ , as follows,

$$\begin{aligned} H_{uv}(\theta, \phi) &= \sum_{m=-\infty}^{\infty} \sum_{n=-\infty}^{\infty} \lambda_{uv}^{(m,n)} e^{i(m\theta+n\phi)}, \quad (u, v = 1, 2, 3), \\ \lambda_{uv}^{(m,n)} &= \frac{1}{4\pi^2} \int_{-\pi}^{\pi} \int_{-\pi}^{\pi} H_{uv}(\theta, \phi) e^{-i(m\theta+n\phi)} d\theta d\phi \quad , \end{aligned} \tag{3}$$

where  $i$  is  $\sqrt{-1}$ .  $\lambda_{uv}^{(m,n)}$  can be numerically integrated by Gaussian quadrature. Thus, the fundamental solution for displacements can also be written as

$$U_{uv}(r, \theta, \phi) = \frac{1}{4\pi r} \sum_{m=-\alpha}^{\alpha} \sum_{n=-\alpha}^{\alpha} \lambda_{uv}^{(m,n)} e^{i(m\theta+n\phi)}, \tag{4}$$

where  $\alpha$  is an integer number, large enough to yield the desired accuracy.

Lee (2009) showed that very high order tensors in the derivatives of the Green's function can be avoided if the partial differentiations are first carried out in the spherical coordinate system and then the chain rule is employed. This was described and explicitly obtained in Shiah, Tan, and Lee (2010). The displacement derivatives can be written in spherical coordinates as

$$U_{ij,l} = \frac{\partial U_{ij}}{\partial r} \frac{\partial r}{\partial x_l} + \frac{\partial U_{ij}}{\partial \theta} \frac{\partial \theta}{\partial x_l} + \frac{\partial U_{ij}}{\partial \phi} \frac{\partial \phi}{\partial x_l}. \tag{5}$$

Carrying out the indicated differentiations in Eq. (5), the partial derivatives of  $U_{ij}$  can be expressed in closed form in terms of the Stroh's eigenvalues (Shiah, Tan, and Lee, 2010; Tan, Shiah, and Wang, 2013). With the partial differentiations carried out on the Fourier series, substituting all previous expressions into Eq. (5) yields

$$U_{ij,l} = \frac{1}{4\pi r^2} \begin{cases} \sum_{m=-\alpha}^{\alpha} \sum_{n=-\alpha}^{\alpha} \lambda_{ij}^{(m,n)} e^{i(m\theta+n\phi)} \begin{bmatrix} -\cos\theta(\sin\phi - in\cos\phi) \\ -imsin\theta/\sin\phi \end{bmatrix} & \text{for } l = 1 \\ \sum_{m=-\alpha}^{\alpha} \sum_{n=-\alpha}^{\alpha} \lambda_{ij}^{(m,n)} e^{i(m\theta+n\phi)} \begin{bmatrix} -\sin\theta(\sin\phi - in\cos\phi) \\ +imcos\theta/\sin\phi \end{bmatrix} & \text{for } l = 2 \\ \sum_{m=-\alpha}^{\alpha} \sum_{n=-\alpha}^{\alpha} \lambda_{ij}^{(m,n)} e^{i(m\theta+n\phi)} [-(\cos\phi + in\sin\phi)] & \text{for } l = 3 \end{cases} \quad (6)$$

where the coefficients  $\lambda_{uv}^{(m,n)}$  are evaluated only once for a given material. Similarly, 2<sup>nd</sup> order derivatives can be obtained by applying the chain rule. All explicit forms are available in Shiah, Tan, and Lee (2010); Tan, Shiah, and Wang (2013).

### 3 Hierarchical Matrices and ACA.

The objective of applying hierarchical matrices and ACA is to reduce the storage requirements as well as to speed up the time required to complete all matrix operations. In this scheme the matrix is represented as a collection of blocks, some of which admit a particular approximated representation that can be obtained by computing only few entries from the original blocks. These special blocks are called low rank blocks. The existence of low rank approximants is based on the asymptotic smoothness of the kernel functions, i.e., on the fact that kernels  $U_{ij}$  and  $T_{ij}$  are singular only when the source and field points are coincident, when  $\mathbf{x} = \mathbf{y}$  (Bebendorf, 2000; Bebendorf and Rjasanow, 2003; Grasedyck, 2005). This is a sufficient condition for the existence of low rank approximants. A low rank block  $M$  of size  $m \times n$  has the following representation

$$M_k = \sum_{i=1}^k a_i \cdot b_i^T = A \cdot B^T \quad (7)$$

where  $A$  is a matrix of size  $m \times k$  and  $B$  is a matrix of size  $n \times k$ . For admissible blocks,  $k$  is low and the representation shown in Eq.(7) requires the storage of  $(m+n)k$  real numbers instead of the  $m \times n$  original block, speeding up the matrix-vector product of the corresponding block. For a detailed analysis refer to Borm, Grasedyck, and Hackbusch (2003); Grasedyck and Hackbusch (2003).

A hierarchical approximation of large dense matrices arising from some generating function having diagonal singularity consists of three basic steps (Kurz, Rain, and Rjasanow, 2007): (i) construction of clusters; (ii) finding of possible admissible blocks; and (iii) low rank approximation of admissible blocks. The construction of clusters was implemented based on the algorithm shown in Kurz, Rain, and Rjasanow (2007). First, the mass and centre of each cluster are stored, and the covariance matrix  $C$  of the cluster is obtained, as follows,

$$C = \sum_{k=1}^n g_k (x_k - X)(x_k - X)^T \quad (8)$$

where  $n$  is the number of elements of the cluster,  $g_k$  is the element area and  $X$  is the centre of the cluster. Then, The eigenvector  $v_1$  corresponding to the largest eigenvalue of  $C$  shows the direction of the largest extension of the cluster. The separation plane goes through the centre  $X$  of the cluster and is orthogonal to  $v_1$ . This algorithm is applied recursively to the sons until they contain less than or equal to some prescribed number  $n_{min}$  of elements. Next, cluster pairs which are geometrically well separated are identified and regarded as admissible cluster pairs. An appropriate admissibility criterion is the following simple geometrical condition. A pair of clusters  $(Cl_x, Cl_y)$  is admissible if

$$\min(\text{diam}(Cl_x), \text{diam}(Cl_y)) \leq \eta \text{dist}(Cl_x, Cl_y), \quad (9)$$

where  $\eta$  is called the admissibility parameter. This parameter influences the number of admissible blocks and the convergence speed of the ACA (Borm, Grasedick, and Hackbusch, 2003). Once the clusters are defined and all admissible blocks are detected, the ACA is applied to approximate by low rank these blocks. Results obtained after the low rank approximation of the admissible blocks by ACA, can be further recompressed, taking advantage of the reduced singular value decomposition (SVD) (Grasedyck, 2005), thereby decreasing the storage requirements. This also serves as a good pre-conditioner for iterative numerical solvers. Some works related to this topic may be found in Benedetti, Milazzo, and Aliabadi (2009); Hackbusch, Khoromskij, and Kriemann (2004).

#### 4 Numerical results.

Three numerical examples are presented to demonstrate the proper implementation of the 3D anisotropic formulation of the Green's function based on Fourier series and the application of the ACA to the BEM analysis. In the first example, a relatively short beam with a square cross-section under pressure load is analyzed. Normalized displacements and direct stresses are compared with the analytical simple

beam theory solution and with the isotropic formulation. The stiffness coefficients were set to match an isotropic material to allow the proper comparison, but the analysis was carried out through the algorithm based on the anisotropic formulation. In the second example, a cube with a cylindrical hole subjected to external pressure is analyzed. The displacement in the  $x_1$  direction is compared with results using the finite element method (FEM). In the third example, an internally pressurized cylinder with a generally anisotropic material is analyzed. The normalized displacement is compared with the results using FEM as reported by Tan, Shiah, and Wang (2013). In the latter two examples, the application of the ACA is tested, and solution times are compared, with the conventional anisotropic BEM formulation. All the computations were performed on a simple PC laptop with a Intel i7-3610QM processor and 8192MB of RAM.

#### 4.1 Example A

The proper implementation of the algorithm for the anisotropic formulation based on Fourier series is first tested. A short beam of length  $2L$  and square cross-section of side  $H$ , where  $L = 5H$ , is subjected to a uniformly distributed pressure load on its top surface, as shown in Fig. 1(b). Both ends of the beam are constrained in the three coordinate directions. Advantage is taken of symmetry and only half the beam was modeled in the BEM analysis, as shown in Fig. 1(a).

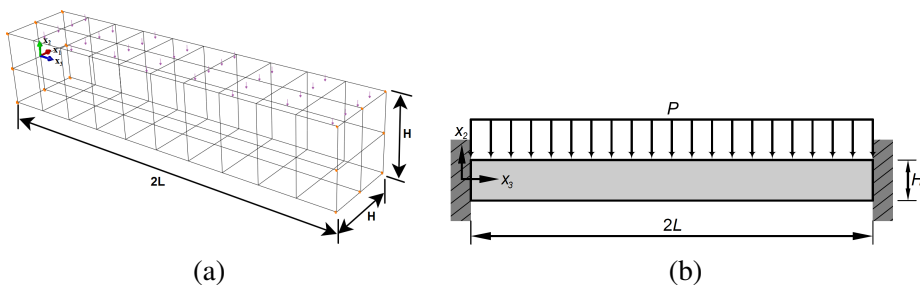


Figure 1: (a) BEM mesh (Symmetry); (b) Equivalent beam model.

A total of 88 quadratic quadrilateral elements and 266 nodes are used to model the problem. For the Fourier series representation,  $\alpha = 16$  and 64 Gauss integration points were used. Normalized transverse displacements along the  $x_3$ -direction are computed and compared with the isotropic BEM formulation and simple beam theory, as shown in Fig. 2. The normalized direct stress is also compared for cross-sections corresponding to  $x_3 = 2H, 3H, 4H, 5H$ , as can be seen in Fig. 3. Even with the coarse BEM mesh, good agreement of the results is observed, with a maximum normalized displacement error of 6.3% at  $x_3 = L$ .

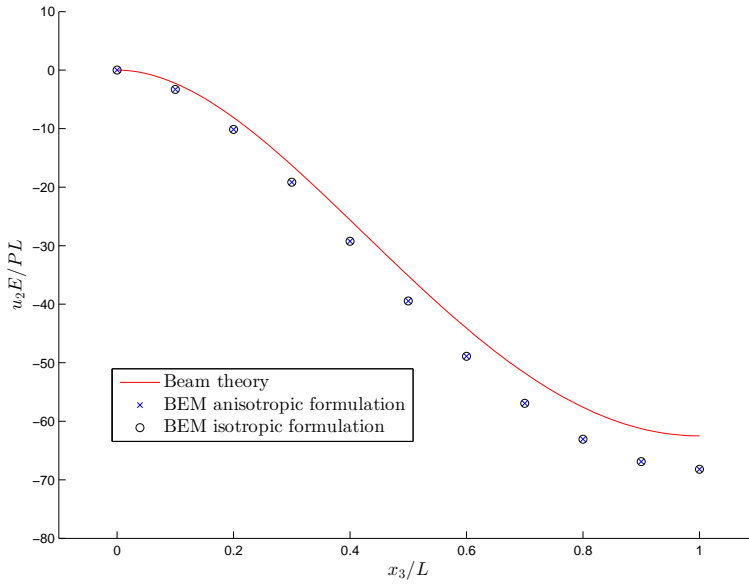


Figure 2: Normalized transverse displacements.

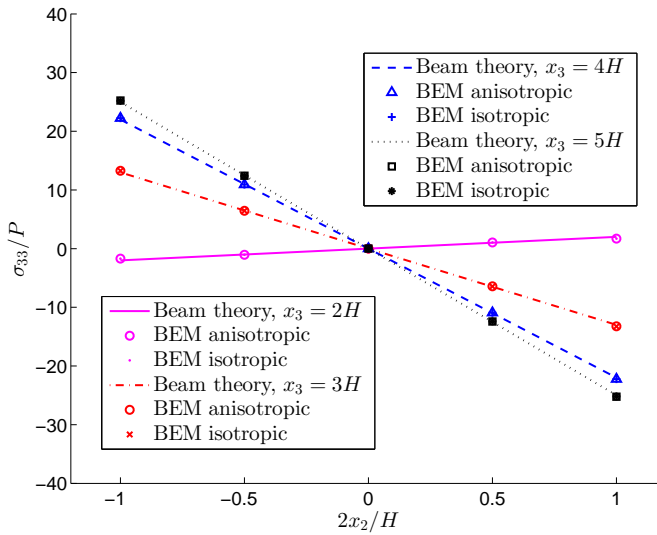


Figure 3: Normalized direct stresses at  $x_1 = 2H, 3H, 4H, 5H$ .

### 4.2 Example B

The physical problem in this second example is a cube with a cylindrical hole. The main objective here is to verify the ACA scheme. The radius of the hole is  $r = 0.3H$ , where  $H$  is the length of its sides, which are subjected to external pressure  $P$ , as shown in Fig. 4(a). The bottom and top surfaces are totally constrained in the three coordinate directions. The material considered is an alpha-quartz with the following stiffness matrix,

$$C = \begin{bmatrix} 87.6 & 6.07 & 13.3 & 17.3 & 0 & 0 \\ 6.07 & 87.6 & 13.3 & -17.3 & 0 & 0 \\ 13.3 & 13.3 & 106.8 & 0 & 0 & 0 \\ 17.3 & -17.3 & 0 & 57.2 & 0 & 0 \\ 0 & 0 & 0 & 0 & 57.2 & 17.3 \\ 0 & 0 & 0 & 0 & 17.3 & 40.765 \end{bmatrix} \text{ GPa} \quad (10)$$

Four different meshes (192, 384, 704 and 1040 quadratic quadrilateral elements) were analyzed. Figure 4(b) shows the coarsest mesh, while Fig. 4(c) shows the most refined one employed.

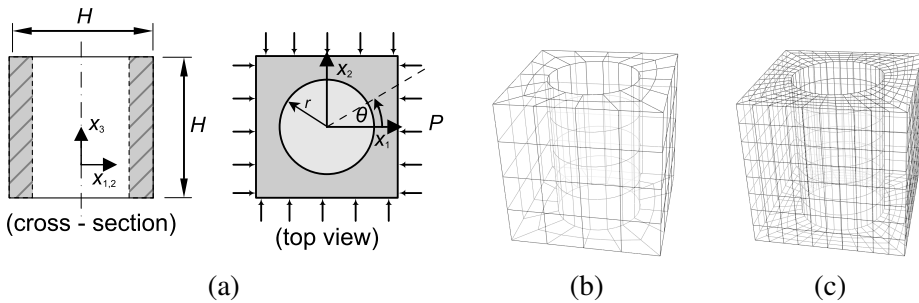


Figure 4: (a) geometry of example B; (b) BEM coarsest mesh; (c) BEM most refined mesh.

The ACA error tolerance is set to  $\epsilon_c = 10^{-4}$ . Moreover, a SVD recompression is involved to create a pre-conditioner matrix for the iterative solver, the generalized minimum residual method (GMRES). The recompression tolerance is set to  $\epsilon_c = 10^{-2}$ . The maximum number of elements per cluster was set to 40 and the admissibility parameter ( $\eta$ ) to 0.8. More details of the choice of these parameters are available in Rodríguez, Sollero, and Albuquerque (2012); Rodríguez, Galvis, Sollero, and Albuquerque (2013); Benedetti, Milazzo, and Aliabadi (2009). For the most refined case (1040 elements) there were 95 clusters and 2304 blocks created,

from which 872 were admissible pairs. Results from the BEM anisotropic formulation using the ACA (for the most refined mesh) are compared with the FEM results obtained by the commercial software Abaqus. The displacement in the  $x_1$  direction on the internal cylindrical surface at  $x_3 = 0.5H$  is compared along the circumferential position  $\theta$ . The results are shown in Fig. 5. The computer cpu times are also compared and are shown in Fig. 6. With the finest mesh, the ACA scheme becomes more efficient computationally in obtaining the same accurate results than the conventional BEM.

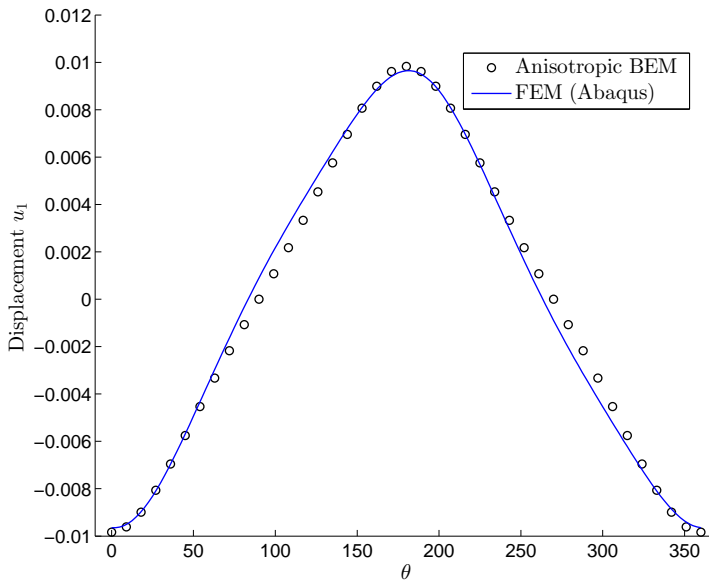


Figure 5: Comparison of the  $u_1$  displacement around the circumferential hole in the mid-plane.

### 4.3 Example C

The physical problem in this third example is an internally pressurized cylinder made of an alpha-quartz crystal, as treated in Tan, Shiah, and Wang (2013). The main objective here is also to verify the ACA scheme when highly anisotropic materials are tested. The problem considered is a cylinder with internal pressure,  $P$ , with radius ratio  $R_2/R_1 = 2$  and total length  $2H = 8R_1$ , as shown in Fig. 7(a). The external circumferential surface is constrained in the radial direction, while its two ends are fixed in the  $x_3$  direction. The principal material axes of the alpha-quartz crystal are successively rotated about the global Cartesian  $x_1$ ,  $x_2$  and  $x_3$  axis

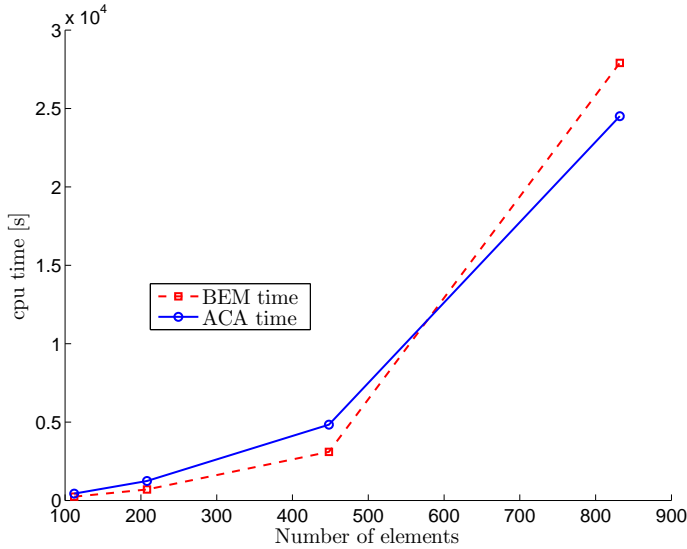


Figure 6: BEM and ACA cpu times.

by  $30^\circ$ ,  $45^\circ$  and  $60^\circ$  clockwise, respectively. These successive rotations yield a fully populated stiffness matrix, as follows,

$$\mathbf{C} = \begin{bmatrix} 111.8 & 14.8 & -5.2 & -0.3 & 11.0 & -14.0 \\ 14.8 & 101.8 & -7.6 & 0.4 & -0.6 & 18.9 \\ -5.2 & -7.6 & 129.7 & 4.4 & 1.6 & 0.6 \\ -0.3 & 0.4 & 4.4 & 31.3 & 2.5 & 3.6 \\ 11.0 & -0.6 & 1.6 & 2.5 & 37.9 & 1.3 \\ -14.0 & 18.9 & 0.6 & 3.6 & 1.3 & 55.2 \end{bmatrix} \text{ GPa} \quad (11)$$

Six different meshes (96, 216, 448, 680, 960 and 1232 quadratic quadrilateral elements) were analyzed. Figure 4(b) shows the coarsest mesh, while Fig. 7(c) shows the most refined one employed.

The ACA error tolerance is set to  $\epsilon_c = 10^{-4}$ . The recompression tolerance is set to  $\epsilon_c = 10^{-2}$ . The maximum number of elements per cluster was set to 60 and the admissibility parameter ( $\eta$ ) to 0.8. For the most refined case (1232 elements) there were 55 clusters and 576 blocks created, from which 96 were admissible pairs. Results from the BEM anisotropic formulation using the ACA (for the most refined mesh) are compared with the FEM results obtained by the commercial software ANSYS, carried out in Tan, Shiah, and Wang (2013). The normalized total

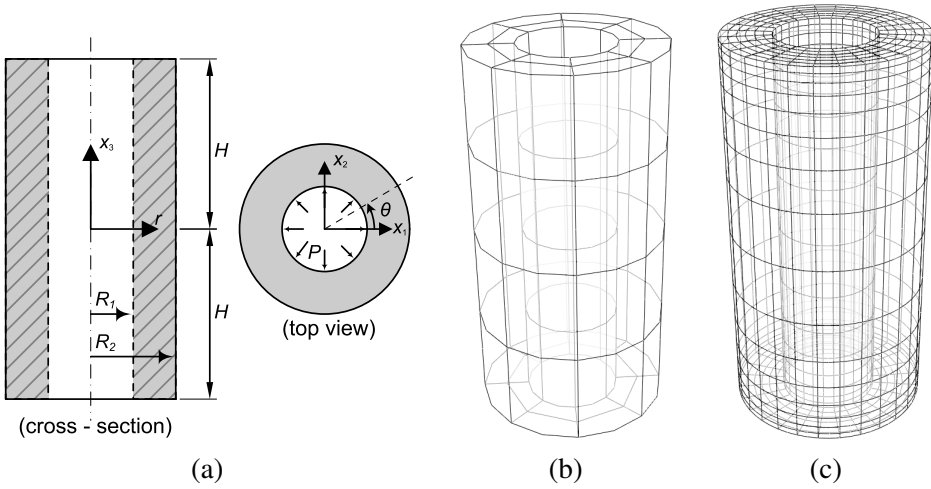


Figure 7: (a) geometry of example C; (b) BEM most refined mesh; (c) BEM coarsest mesh.

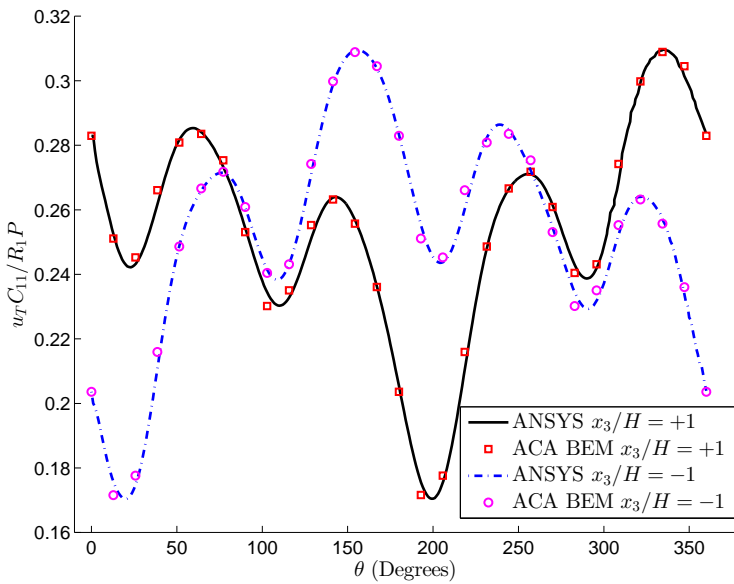


Figure 8: Normalized total displacement comparison.

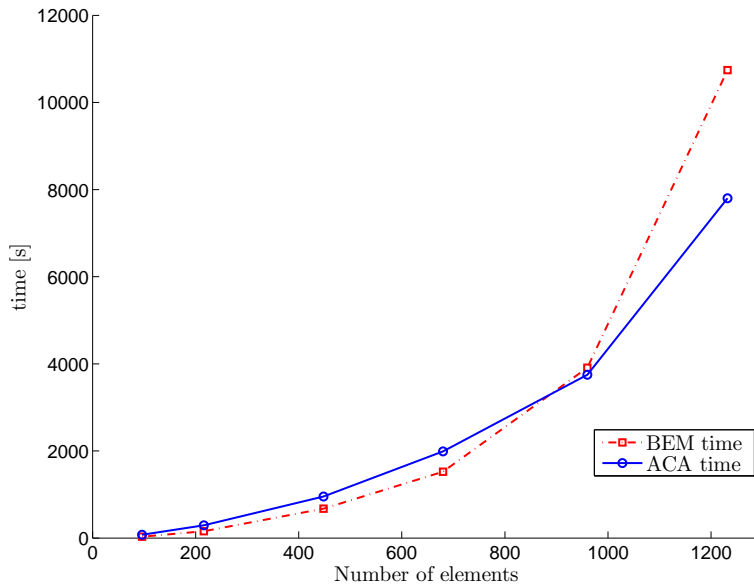


Figure 9: BEM and ACA cpu times.

displacement ( $u_T C_{11}/PR_1$ ) at  $r = 1.5R_1$  on both ends is compared along the circumferential position  $\theta$ . The results are shown in Fig. 8. The cpu times are also compared and are shown in Fig. 9. Again, with high number of elements, the ACA scheme takes less cpu times than the conventional BEM.

## 5 Conclusions.

In this work, the use of hierarchical matrices and low-rank approximations applied to the anisotropic 3D formulation based on Fourier series has been presented. Low rank approximations were accomplished by the use of ACA. This method is suitable for memory and time savings, especially in the case of large-scale problems. The ACA works better beyond a certain number of elements in the mesh. After this point the solution time reported by the ACA will be less than the conventional BEM formulation.

**Acknowledgement:** The authors would like to thank the Sao Paulo Research Foundation (FAPESP) for the financial support.

## References

- Bebendorf, M.** (2000): Approximation of boundary element matrices. *Numerische Mathematik*, vol. 86, pp. 565 – 589.
- Bebendorf, M.; Rjasanow, S.** (2003): Adaptive low-rank approximation of collocation matrices. *Computing*, vol. 70, pp. 1 – 24.
- Benedetti, I.; Milazzo, A.; Aliabadi, M.** (2009): A fast dual boundary element method for 3D anisotropic crack problems. *International Journal for Numerical Methods in Engineering*, vol. 80, pp. 1356 – 1378.
- Borm, S.; Grasedyck, L.; Hackbusch, W.** (2003): Introduction to hierarchical matrices with applications. *Engineering Analysis with Boundary Elements*, vol. 27, pp. 405–422.
- Brancati, A.; Aliabadi, M.; Benedetti, I.** (2009): Hierarchical adaptive cross approximation GMRES technique for solution of acoustic problems using the boundary element method. *CMES: Computer Modeling in Engineering & Sciences*, vol. 43, pp. 149–172.
- Brancati, A.; Aliabadi, M.; Milazzo, A.** (2011): An improved hierarchical ACA technique for sound absorbent materials. *CMES: Computer Modeling in Engineering & Sciences*, vol. 78, pp. 1–24.
- Grasedyck, L.** (2005): Adaptive recompression of H–matrices for BEM. *Computing*, vol. 74, pp. 205–223.
- Grasedyck, L.; Hackbusch, W.** (2003): Construction and arithmetics of H–matrices. *Computing*, vol. 70, pp. 295–334.
- Hackbusch, W.; Khoromskij, B.; Kriemann, R.** (2004): Hierarchical matrices based on weak admissibility criterion. *Computing*, vol. 73, pp. 207–243.
- Kurz, S.; Rain, O.; Rjasanow, S.** (2007): *Fast boundary element methods in computational Electromagnetism*. Springer.
- Lee, V.** (2003): Explicit expression of derivatives of elastic Green’s functions for general anisotropic materials. *Mech. Res. Comm.*, vol. 30, pp. 241–249.
- Lee, V.** (2009): Derivatives of the three-dimensional Green’s function for anisotropic materials. *International Journal for Solids and Structures*, vol. 46, pp. 3471–3479.
- Rodríguez, R.; Galvis, A. F.; Sollero, P.; Albuquerque, E.** (2013): Analysis of multiple inclusion potential problems by the adaptive cross approximation method. *CMES: Computer Modeling in Engineering & Sciences*, vol. 96, pp. 259–274.

**Rodríguez, R.; Sollero, P.; Albuquerque, E.** (2012): Analysis of anisotropic symmetric plates by the adaptive cross approximation. In *Advances in Boundary Element & Meshless Techniques*, pp. 303–310.

**Rokhlin, H.** (1985): Rapid solution of integral equation of classical potential theory. *Journal of Computational Physics*, vol. 60, pp. 187–207.

**Shiah, Y. C.; Tan, C. L.; Lee, R. F.** (2010): Internal point solutions for displacements and stresses in 3D anisotropic elastic solids using the boundary element method. *CMES: Computer Modeling in Engineering & Sciences*, vol. 69, pp. 167–197.

**Shiah, Y. C.; Tan, C. L.; Wang, C. Y.** (2012): Efficient computation of the Green's function and its derivatives for three-dimensional anisotropic elasticity in BEM analysis. *Engineering Analysis with Boundary Elements*, vol. 36, pp. 1746–1755.

**Tan, C.; Shiah, Y.; Lin, C.** (2009): Stress analysis of 3D generally anisotropic elastic solids using the boundary element method. *CMES: Computer Modeling in Engineering & Sciences*, vol. 41, pp. 195–214.

**Tan, C. L.; Shiah, Y. C.; Wang, C. Y.** (2013): Boundary element elastic stress analysis of 3D generally anisotropic solids using fundamental solutions based on Fourier series. *International Journal of Solids and Structures*, vol. 50, pp. 2701–2711.

**Ting, T.; Lee, V.** (1997): The three-dimensional elastostatic Green's function for general anisotropic linear elastic solids. *J. Mech. Appl. Math.*, vol. 50, pp. 407–426.

**Wang, H.; Yao, Z.** (2013): ACA-accelerated time domain BEM for dynamic analysis of HTR-PM nuclear island foundation. *CMES: Computer Modeling in Engineering & Sciences*, vol. 94, pp. 507–527.

**Wang, P. B.; Yao, Z. H.; Lei, T.** (2006): Analysis of solids with numerous micro-cracks using the fast multipole DBEM. *CMC: Computers, Materials & Continua*, vol. 3 (2), pp. 65–76.

**Wang, Q.; Zhu, Y. M. H. P.; Zhang, C.** (2012): An  $O(N)$  fast multipole hybrid boundary node method for 3D elasticity. *CMC: Computers, Materials & Continua*, vol. 28 (1), pp. 1–26.

**Yoshikawa, H.; Matsumura, R.; Nishimura, N.** (2013): Time domain biem with cqm accelerated with aca and truncation for the wave equation. *CMES: Computer Modeling in Engineering & Sciences*, vol. 94, pp. 553–565.